

1 **Backwater controls on the sedimentology, kinematics and geometry of bar deposits in coastal rivers**

2 Anjali M. Fernandes¹, Virginia B. Smith², Kashauna G. Mason³

3 ¹The Center for Integrative Geosciences, The University of Connecticut, 354 Mansfield Road, Unit 1045,
4 Storrs, Connecticut 06269, U. S. A. Email: anjali.fernandes@uconn.edu

5 ²Villanova University 800 Lancaster Avenue Villanova, PA, 190851603, U. S. A.

6 ³Department of Geosciences, 340 N. Campus Drive, 216 Gearhart Hall, University of Arkansas,
7 Fayetteville, AR 72701, U. S. A.

8 **Abstract**

9 **The backwater reach of coastal rivers is associated with considerable spatial and temporal**
10 **variability in water and sediment flux. Here we test the hypothesis that the spatial and temporal**
11 **variability in water flux and particle sizes in transport are expressed as systematic changes in the**
12 **geometry of bank-attached bars across the backwater transition. Measured transverse slopes of**
13 **bank-attached bars in the Mississippi and Trinity Rivers show a systematic increase as the river**
14 **transitions from normal flow to the backwater. To explain this trends, we use a simple force balance**
15 **relationship, in which the transverse slope of the bars constructed through traction transport varies**
16 **in proportion to the square of depth-averaged flow velocity and is inversely proportional to the**
17 **square of the median particle size of the supplied sediment, in bends with similar curvature. The**
18 **observed trend is therefore explained by a downstream reduction in particle sizes coupled with a**
19 **downstream increase in flow velocity across the backwater transition at high discharge, during which**
20 **sand fluxes are greatest.**

21 **Introduction**

22 River deposits in the coastal backwater zone display considerable spatial heterogeneity. This is
23 likely the result of spatial and temporal non-uniformity in influences from upstream (e.g. water discharge,
24 sediment flux) as well as downstream (e.g. sea-level, river plume dynamics). Constraining the fundamental
25 controls on the complex geometries of sedimentary strata built by coastal rivers is essential for: (a)
26 reconstructing Earth's past environments from shelf margin deposits, (b) characterizing reservoir properties

27 in shallow or deep subsurface environments, where channel deposits are the primary pathways for transport
28 of fluids and contaminants (Kolker et al., 2013; Sawyer et al., 2015; Martin et al., 2018), and (c)
29 constraining surface dynamics in data-limited settings on Earth or other planetary bodies.

30 Backwater zones occur in the terminal reaches of rivers, where they meet a standing body of water
31 in oceans or lakes (Chow, 1959). The length of the backwater zone (L_b) is estimated as $L_b \approx H/S$, where H
32 is mean flow depth and S is the gradient of the water surface (Paola and Mohrig, 1996; Fig. 1). At the
33 backwater transition, gravity-driven, normal flow conditions give way to temporally and spatially varying
34 hydraulic conditions where both gravity and pressure gradients are important (Lane, 1957). As indicated
35 by a number of recent studies, backwater hydrodynamics can influence sediment transport dynamics, the
36 morphodynamics of rivers and floodplains, the position of delta avulsion nodes, as well as depositional
37 trends over millennial to million-year timescales (Jerolmack and Swenson, 2007; Petter, 2010; Nittrouer et
38 al., 2011a, 2011b, 2012; Lamb et al., 2012; Smith, 2012; Chatanantavet et al., 2012; Blum et al., 2013;
39 Ganti et al., 2014, 2016; Fernandes et al., 2016; Mason and Mohrig, 2018; Trower et al., 2018; Martin et
40 al., 2018).

41 The transition from normal flow to backwater-influenced flow (Fig. 1) in the Lower Mississippi
42 River (LMR) occurs at approximately 600-750 river kilometers (RK; $H=10-30$ m, $S=10^{-5}$; Nittrouer et al.,
43 2012). Studies of flow and sediment transport through the LMR reveal that flow decelerates downstream
44 during low or moderate discharge ($<3 \times 10^4$ m³/s) and the terminal segment of the LMR acts as a “settling
45 basin”, accumulating a thick mantle of mud over channel bed and side-walls (Nittrouer et al., 2011a, 2012;
46 Fig. 1). At high discharge ($>3 \times 10^4$ m³/s), the water level rises in the normal flow reach but remains relatively
47 fixed near the river mouth, causing a downstream acceleration of flow and associated increase in bed
48 material flux by two orders of magnitude across the lower RK200 (Nittrouer et al., 2012). During high-
49 discharge events, easily suspended particles <0.3 mm in diameter sand are transported through the
50 backwater zone and similarly partitioned between bedload and suspended load, whereas >0.4 mm sand
51 particles are thought to be transported as relatively slow-moving bedload within the upper backwater zone
52 (Wright and Parker, 2005; Nittrouer, 2013). These observations of sand-transport through the lower MR

53 lead to the inference that bar construction is primarily associated with high discharge events, as this is the
54 only time sand moves through the backwater zone. Here we test the hypothesis that spatio-temporal
55 variability in flow and sediment transport result in consistent spatial patterns in bank-attached bar
56 geometries, kinematics and sedimentology in the backwater zones of coastal rivers.

57 **The Balance of Forces Controlling the Transverse Slopes of Bars Constructed by Traction Load**

58 The transverse slope of a bar across which active bedload transport occurs is set by a balance of
59 forces: (1) the gravitational pull on the particle, acting in the downslope direction, and (2) the force acting
60 up the bar, induced by cross-stream circulation in bends (Dietrich and Smith, 1984; Sekine and Parker,
61 1992). The force F_d acting on individual sediment grains with diameter D as they are transported
62 downstream across the transverse bar slope θ can be expressed as:

$$63 \quad F_d = \rho' g \pi \frac{1}{4} D^2 \sin\theta \quad (1)$$

64 Where ρ' is the submerged density of silica sand in water and g is gravitational acceleration. This may also
65 be expressed as:

$$66 \quad F_d \propto D^2 \sin\theta \quad (2)$$

67 When a resisting force exerted by the component of helical flow acting up the sloping bar surface balances
68 the effect of gravity, saltating sediment particles will move downstream across the transverse slope instead
69 of towards the thalweg (Dietrich and Smith, 1984; Sekine and Parker, 1992). This force is related to flow
70 velocity and the radius of curvature of the bend (Komar, 1969) as in:

$$71 \quad F_r \propto \rho \frac{u^2}{R_c} \quad (3)$$

72 Where R_c is the radius of curvature of the channel, ρ is the density of the fluid and u is the depth-averaged
73 flow velocity.

74 When the forces are balanced,

$$75 \quad \sin\theta \propto \frac{u^2}{D^2 R_c} \quad (4)$$

76 Therefore, for bends of a given curvature, cross-channel bar slope varies in proportion to (1) the square of
77 the characteristic velocity associated sediment transport at high discharge through bends in the backwater

78 zone and (2) the inverse of the representative particle size in traction load squared. Thus, if the depth-
79 averaged flow velocity increases downstream across the backwater zone and particle sizes available for bar
80 construction decrease, this relationship predicts a downstream increase in the transverse slopes of bars.

81 **Bank-attached Bar Composition and Geometry across the Backwater Zone of the Mississippi River**

82 We present spatial patterns in geometry and composition using data from 1265 borehole logs
83 compiled by the U.S. Army Corps of Engineers (USACE) in the Late Holocene Mississippi channel belt
84 (MCB; Fig. 1b) (Saucier, 1994; Fernandes et al., 2016), grain-size data of bed material from the modern
85 MR (USACE, 1935) and bathymetry collected in 1913 (See Data Repository (DR)). These data sources
86 pre-date significant engineering modification to the MR channel, though we acknowledge that some
87 anthropogenic impact may manifest even in these data. Sedimentary facies from boreholes, which represent
88 millennial-scale sedimentation patterns, were used to characterize bulk facies changes across the backwater
89 zone. We used: (A) mud- rich residual channel fills as proxies for MCB thickness (Fernandes et al., 2016),
90 (B) sand and mud deposited at the tops of point bars as proxies for easily-suspended sediment load, and (C)
91 a mix of sand and gravel beneath Facies B, interpreted as the undifferentiated deposits of bedload-
92 dominated MCB point bars and underlying Pleistocene braided rivers. Downstream of RK400, where
93 oxbow lakes are absent, the thickness of Facies B was used as a proxy for MCB thickness (Fernandes et al.,
94 2016); between RK300-RK400, only thicknesses that exceeded the p75 of Facies B were used. A
95 comparison of the two sets of measurements provided a proxy for the contribution of easily suspended
96 material to MCB bars, from just downstream of Cairo, Illinois (RK1250) to Head of Passes (RK0) (Fig.
97 2A). Downstream of RK500, the MCB thickens and bars incorporate increasing amounts of Facies B,
98 which dominates channel-belt deposits between RK0 and RK200. The bed material load (Fig. 2B) grows
99 enriched in particle sizes <0.3 mm (medium grained sand) downstream of RK200, the likely result of long-
100 term storage of “perennial” bedload (>0.4 mm) in the upper backwater zone (U. S. Army Corps of
101 Engineers, 1935). Notably, the limit of the slow-moving gravel front occurs in the vicinity of RK400, near
102 Baton Rouge (Nittrouer, 2013, Fig. 2B).

103 We measured the cross-channel slopes of bank-attached bars (Fig. 2C, E, F) as well as the planform
104 shape of the bar surfaces using the bathymetric data from RK500 to RK0. The percentiles (p) of
105 measurements within a RK100 show increases (Fig. 2C, E) from upstream of RK400 (p10=1°, p25=2°,
106 p50=3°, p75=4°, p90=5°) to downstream of RK300 (p10=2.5°, p25=3°, p50=4°, p75=4.5°-5.5°; p90=6°-
107 7.5°); distributions also become increasingly skewed towards higher slopes downstream of RK350.
108 Suspension-dominated sediment deposition, in flow-separation zones downstream of high curvature bends
109 or point bars, can display very high slopes (Smith et al., 2009). We evaluated the curvature of bars in context
110 of the transverse slopes (Fig. 2D). Curvatures of bar deposits, expressed as the inverse of radii of curvature
111 and assigned different signs depending on whether they were convex or concave with respect to the channel
112 centerline (Fig. 2F), do not show any systematic spatial trend in the relative abundance of these shapes.
113 Therefore, backwater dynamics do appear to cause a systematic increase in transverse bar slopes; the
114 distributions of planform curvatures of bars, however, appear unaffected within the studied reach.

115 **Linking the Kinematics and Geometry of Bars across the Backwater Zone of the Mississippi and** 116 **Trinity Rivers**

117 In the past, authors have hypothesized that downstream changes in channel lateral migration rates
118 are linked to spatially variable sediment storage in bars and cross-stream bar geometry (Ikeda, 1989; Smith,
119 2012; Nittrouer et al., 2012; Blum et al., 2013; Fernandes et al., 2016). We test this idea by comparing the
120 transverse bar slopes and lateral migration rates (Fig.3) of two alluvial rivers: 1) the Lower Trinity River
121 (LTR), Texas, (Smith, 2012; Smith and Mohrig, 2017; Mason and Mohrig, 2018; Smith et al., in review),
122 2) the LMR (Hudson and Kesel, 2000). The LTR is a sand-bedded river with an insignificant amount of
123 engineered modification in the studied region. Sediment samples from bars across the backwater zone
124 reveal uniform distributions of sand-sized (<1.5 mm) sediment; however, gravel-sized particles, observed
125 in samples from near the backwater transition, are absent from the samples in the lower backwater zone
126 (Smith, 2012; Smith et al., in review). Both rivers have bathymetry collected over the required river channel
127 length to compute the cross-channel slopes of bars and sufficient time-lapse information to compute lateral
128 channel migration rates respectively.

129 To account for their different scales, we divided distances upstream of the terminus of the LMR
130 and LTR by the respective backwater lengths of each river (700 km and 50 km) and lateral migration rates
131 by the mean channel width in the backwater zone (70 m and 90 m; Smith, 2012; Nittrouer et al., 2012).
132 Transverse slopes of bars in both rivers follow similar trends; they show a systematic increase downstream
133 of the backwater transition in both rivers (Fig. 3). This is likely to be in response to downstream fining of
134 bed material (Smith, 2012; Smith et al., in review) and/or downstream acceleration at high discharge.
135 Channel migration rates for both rivers increase at the normal flow to backwater transition (dimensionless
136 distance = 1) but decrease drastically downstream across the backwater zone (Fig. 2). This is probably a
137 consequence of sand storage at the backwater transition (Nittrouer et al., 2012; Smith, 2016; Fernandes et
138 al., 2016). Channel asymmetry in normal flow, associated with prolific bar growth and shallower cross-
139 channel slopes at the backwater transition, likely contributes to topographic steering of high-velocity flow,
140 enhanced erosion of the outer bank and locally accelerated lateral migration (Ikeda et al., 1981; Eke et al.,
141 2014).

142 **Discussion**

143 The systematic and predictable increase in the cross-stream slopes of the two studied rivers and
144 reduction in particle size of sediment, coupled with a reduction in the lateral migration rates downstream
145 of the backwater transition zone, indicate that the dynamics of flow and sediment transport across the
146 backwater zone have a fundamental impact on the kinematics, composition and geometry of bank-attached
147 bars (Ikeda, 1989; Smith, 2012; Nittrouer et al., 2012; Fernandes et al., 2016). Furthermore, the proposed
148 force balance scaling likely represents a sound first step towards explaining observed trends in cross-
149 channel bar slopes through the backwater zone. Figures 2 A, B and C offer the intriguing opportunity for
150 connecting (1) the spatio-temporal non-uniformity in sediment-transport dynamics, to (2) the spatial
151 variability of sedimentary facies, in terms of relative sand and mud content, and (3) the dip of preserved
152 bar accretion sets in the sedimentary record of fluvial backwater zones. This is particularly relevant to
153 paleo-environmental reconstructions in data-limited settings. At the scale of rock outcrops, the sedimentary
154 record of laterally mobile channels is dominated by inclined bed-sets formed through bar accretion

155 (Colombera et al., 2017; Durkin et al., 2017; Mahon and McElroy, 2018). Statistically robust spatial trends
156 in the steepness of dipping bar surfaces and the relative proportions of sand and mud in coastal channel
157 belts may serve to locate outcrops along proximal-to-distal paleo-river profiles. The distribution of slopes
158 in the preserved remnants of bar surfaces, however, may be somewhat different from that observed in
159 modern channels. To our knowledge, a formal statistical treatment of this preservation bias has not yet been
160 attempted and may be needed to further quantify uncertainties associated with these trends in the
161 sedimentary record.

162 The current work adds to a growing body of research in which a unifying hydraulic framework is
163 used to elucidate the expected spatial variability in (1) the large-scale geometry of channel belts (i.e.
164 thickness and width), (2) the sedimentary facies, (3) the expected scales of channel bed scours, and (4)
165 geometry of bar deposits filling channel belts, in backwater-influenced paleo-channels (Petter, 2010; Blum
166 et al., 2013; Fernandes et al., 2016; Trower et al., 2018; Martin et al., 2018). These attributes, applicable at
167 different scales of investigation (e.g. remotely sensed channel belts, outcrops or sediment cores), can be
168 used to reconstruct past environments and dynamics of fluvio-deltaic systems on Earth or other planetary
169 bodies (e.g., Goudge et al., 2018) and to predict sub-surface heterogeneity and reservoir potential (e.g.,
170 Durkin et al., 2017; Milliken et al., 2018).

171 **Conclusions**

172 Our comparison of trends in the Lower Mississippi and Lower Trinity Rivers suggests that
173 backwater hydrodynamics and sediment transport dynamics constitute fundamental controls on the
174 sedimentology, geometry and kinematics of bars observed in these systems. These results therefore define
175 a critical link between backwater dynamics and bed-scale stratal geometries, providing a process-based
176 framework for reconstructing paleo-dynamics and -environment from ancient sedimentary strata on Earth
177 and other planets and for predicting reservoir-scale attributes in remotely sensed settings.

178 **Acknowledgements**

179 The authors would like to acknowledge the efforts of the many scientists working for the Trinity River
180 Authority, Texas Parks and Wildlife and the U.S. Army Corps of Engineers who collected much of the data
181 used in this paper.

182 **References Cited**

183 Blum, M., Martin, J., Milliken, K., and Garvin, M., 2013, Paleovalley systems: insights from Quaternary
184 analogs and experiments: *Earth-Science Reviews*, v.116, p. 128 – 169.

185 Chatanantavet, P., Lamb, M.P., and Nittrouer, J.A., 2012, Backwater controls of avulsion location on
186 deltas: *Geophysical research letters*, v. 39, p. L01402, doi: 10.1029/2011GL050197.

187 Colombera, L., Mountney, N.P., Russell, C.E., Shiers, M.N., and McCaffrey, W.D., 2017, Geometry and
188 compartmentalization of fluvial meander-belt reservoirs at the bar-form scale: Quantitative insight
189 from outcrop, modern and subsurface analogues: *Marine and Petroleum Geology*, v. 82, p. 35–55,
190 doi:10.1016/j.marpetgeo.2017.01.024.

191 Dietrich, W.E., and Smith, J.D., 1984, Bed Load Transport in a River Meander: *Water resources research*,
192 v. 20, p. 1355–1380, doi:10.1029/WR020i010p01355.

193 Durkin, P.R., Boyd, R.L., and Hubbard, S.M., 2017, Three-dimensional reconstruction of meander-belt
194 evolution, Cretaceous McMurray formation, Alberta Foreland Basin, Canada: *Journal of*
195 *Sedimentary Research*, v.87, p.1075-1099, doi: 10.2110/jsr.2017.59

196 Eke, E., Parker, G., and Shimizu, Y., 2014, Numerical modeling of erosional and depositional bank
197 processes in migrating river bends with self-formed width: Morphodynamics of bar push and bank
198 pull: *Journal of Geophysical Research: Earth Surface*, v. 119, p. 1455–1483,
199 doi:10.1002/2013JF003020

200 Fernandes, A.M., Törnqvist, T.E., and Straub, K.M., 2016, Connecting the backwater hydraulics of
201 coastal rivers to fluvio-deltaic sedimentology and stratigraphy, v. 44, p. 979–982, doi:

202 10.1130/G37965.1

203 Ganti, V., Chadwick, A.J., Hassenruck-Gudipati, H.J., Fuller, B.M., and Lamb, M.P., 2016, Experimental
204 river delta size set by multiple floods and backwater hydrodynamics: *Science advances*, v. 2, p.
205 e1501768, doi:10.1126/sciadv.1501768.

206 Ganti, V., Chu, Z., Lamb, M.P., Nittrouer, J.A., and Parker, G., 2014, Testing morphodynamic controls
207 on the location and frequency of river avulsions on fans versus deltas: Huanghe (Yellow River),
208 China: *Geophysical research letters*, v. 41, p. 2014GL061918, doi:10.1002/2014GL061918.

209 Goudge, T.A., Mohrig, D., Cardenas, B.T., Hughes, C.M., and Fassett, C.I., 2018, Stratigraphy and
210 paleohydrology of delta channel deposits, Jezero crater, Mars: *Icarus*, v. 301, p. 58–75,
211 doi:10.1016/j.icarus.2017.09.034.

212 Hudson, P.F., and Kesel, R.H., 2000, Channel migration and meander-bend curvature in the lower
213 Mississippi River prior to major human modification: *Geology*, v. 28, p. 531–534,
214 doi:10.1130/0091-7613(2000)28<531:CMAMCI>2.0.CO;2.

215 Ikeda, H., 1989, Channel Migration and Point bar origin in sandy meanders, *in* Ikeda, S. and Parker, G.
216 eds., *River Meandering*, American Geophysical Union, p. 51–68.

217 Ikeda, S., Parker, G., and Sawai, K., 1981, Bend theory of river meanders. Part 1. Linear development:
218 *Journal of Fluid Mechanics*, v.112, p. 363-377.

219 Jerolmack, D.J., and Swenson, J.B., 2007, Scaling relationships and evolution of distributary networks on
220 wave-influenced deltas: *Geophysical Research Letters*, v. 34, doi:10.1029/2007GL031823.

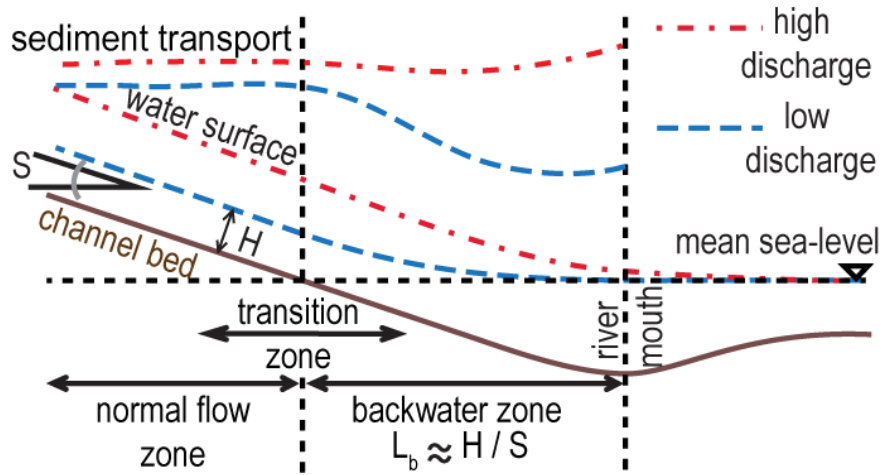
221 Kolker, A.S., Cable, J.E., Johannesson, K.H., and Allison, M.A., 2013, Pathways and processes
222 associated with the transport of groundwater in deltaic systems: *Journal of Hydrology*, v. 498, p.
223 319-334, doi: 10.1016/j.jhydrol.2013.06.014

- 224 Komar, P.D., 1969, The channelized flow of turbidity currents with application to Monterey Deep-Sea
225 Fan Channel: *Journal of geophysical research*, v. 74, p. 4544–4558, doi:10.1029/JC074i018p04544.
- 226 Lamb, M.P., Nittrouer, J.A., Mohrig, D., and Shaw, J., 2012, Backwater and river plume controls on
227 scour upstream of river mouths: Implications for fluvio-deltaic morphodynamics: *Journal of*
228 *Geophysical Research: Earth Surface*, v. 117, F01002, doi:10.1029/2011JF002079.
- 229 Lane, E. W., 1957, *A Study of the Shape of Channels Formed by Natural Streams Flowing in Erodible*
230 *Material*, U.S. Army Corps of Engineers, Mo. River Div., Omaha, Nebr.
- 231 Mahon, R.C., and McElroy, B., 2018, Indirect estimation of bedload flux from modern sand-bed rivers
232 and ancient fluvial strata: *Geology*, v. 46, p. 579–582. doi:10.1130/G40161.1.
- 233 Martin, J., Fernandes, A.M., Pickering, J., Howes, N., Mann, S., and McNeil, K., 2018, The
234 Stratigraphically Preserved Signature of Persistent Backwater Dynamics in a Large Paleodelta
235 System: The Mungaroo Formation, North West Shelf, Australia: *Journal of Sedimentary Research*,
236 v. 88, p. 850–872, doi:10.2110/jsr.2018.38.
- 237 Mason, J., and Mohrig, D., 2018, Using time-lapse lidar to quantify river bend evolution on the
238 meandering coastal Trinity River, Texas, USA: *Journal of Geophysical Research: Earth Surface*, v.
239 123, 1133–1144. Doi:10.1029/ 2017JF004492
- 240 Milliken, K.T., Blum, M.D., Snedden, J.W., and Galloway, W.E. Application of fluvial scaling
241 relationships to reconstruct drainage-basin evolution and sediment routing for the Cretaceous and
242 Paleocene of the Gulf of Mexico: *Geosphere*, v. 14, p. 1–19,
243 doi:10.1130/GES01374.1.doi:10.1130/GES01374.1.
- 244 Nittrouer, J.A., 2013, Backwater hydrodynamics and sediment transport in the lowermost Mississippi
245 River Delta: Implications for the development of fluvial-deltaic landforms in a large lowland river:
246 *Deltas: Landforms, Ecosystems, and Human Activities: International Association of Hydrological*

- 247 Sciences Publication, v. 358, p. 48–61.
- 248 Nittrouer, J.A., Mohrig, D., and Allison, M., 2011a, Punctuated sand transport in the lowermost
249 Mississippi River: *Journal of Geophysical Research*, v. 116, p. F04025, doi:10.1029/2011JF002026.
- 250 Nittrouer, J.A., Mohrig, D., Allison, M.A., and Peyret, A.-P.B., 2011b, The lowermost Mississippi River:
251 a mixed bedrock-alluvial channel: *Sedimentology*, v. 58, p. 1914–1934, doi:10.1111/j.1365-
252 3091.2011.01245.x.
- 253 Nittrouer, J.A., Shaw, J., Lamb, M.P., and Mohrig, D., 2012, Spatial and temporal trends for water-flow
254 velocity and bed-material sediment transport in the lower Mississippi River: *GSA Bulletin*, v. 124, p.
255 400–414, doi:10.1130/B30497.1.
- 256 Paola, C., and Mohrig, D., 1996, Palaeohydraulics revisited: palaeoslope estimation in coarse-grained
257 braided rivers: *Basin Research*, v. 8, p. 243–254, doi:10.1046/j.1365-2117.1996.00253.x.
- 258 Petter, A.L., 2010, Stratigraphic implications of the spatial and temporal variability in sediment transport
259 in rivers, deltas, and shelf margins [Ph.D. thesis]: Austin, University of Texas at Austin, 205 p.
- 260 Saucier, R.T., 1994, *Geomorphology and Quarternary Geologic History of the Lower Mississippi Valley*.
261 Volume 2: AU. S. Army Corps of Engineers, Waterways Experiment Station.
- 262 Sawyer, A.H., Edmonds, D.A., and Knights, D., 2015, Surface water-groundwater connectivity in deltaic
263 distributary channel networks: *Geophysical Research Letters*, v. 42, p. 10,299–10,306,
264 doi:10.1002/2015GL066156.
- 265 Sekine, M., and Parker, G., 1992, Bed-load transport on transverse slope. I: *Journal of Hydraulic*
266 *Engineering*, v. 118, p. 513–535, doi:10.1061/(ASCE)0733-9429(1992)118:4(513).
- 267 Smith, V.B., 2012, *Geomorphology of a coastal sand-bed river: Lower Trinity River, Texas* [Ph.D.
268 thesis]: Austin, University of Texas at Austin

- 269 Smith, D.G., Hubbard, S.M., Leckie, D.A., and Fustic, M., 2009, Counter point bar deposits: lithofacies
270 and reservoir significance in the meandering modern Peace River and ancient McMurray Formation,
271 Alberta, Canada: *Sedimentology*, v. 56, p. 1655–1669, doi:10.1111/j.1365-3091.2009.01050.x.
- 272 Smith, V.B., and Mohrig, D., 2017, Geomorphic signature of a dammed Sandy River: The lower Trinity
273 River downstream of Livingston Dam in Texas, USA: *Geomorphology*, v.297, p. 122-136.
- 274 Smith, V.B., Mason, J., and Mohrig, D., Morphodynamics of a Backwater Influenced Sand-bed River:
275 The Lower Trinity River, Texas, USA, *in review*, *Earth and Planetary Science Letters*.
- 276 Chow, V. T., 1959, *Open-channel hydraulics*: McGraw-Hill New York, v. 1.
- 277 Trower, E.J., Ganti, V., Fischer, W.W., and Lamb, M.P., 2018, Erosional surfaces in the Upper
278 Cretaceous Castlegate Sandstone (Utah, USA): Sequence boundaries or autogenic scour from
279 backwater hydrodynamics? *Geology*, v. 46, p. 707-710. doi:10.1130/G40273.1.
- 280 U. S. Army Corps of Engineers, 1935, *Studies of River Bed Materials and their Movement, with Special*
281 *Reference to the Lower Mississippi River*: U. S. Army Corps of engineers, Waterways Experiment
282 Station Paper 17.
- 283 Wright, S., and Parker, G., 2005, Modeling downstream fining in sand-bed rivers. I: formulation: *Journal*
284 *of Hydraulic Research*, v. 43, p. 613–620, doi:10.1080/00221680509500381.
- 285

286 **Figures and Captions**



287

288 Figure 1: Schematic summary of spatial and temporal patterns in water surface slope, predicted sediment
289 transport trends (from Nittrouer et al., 2012) and terminology used.

290

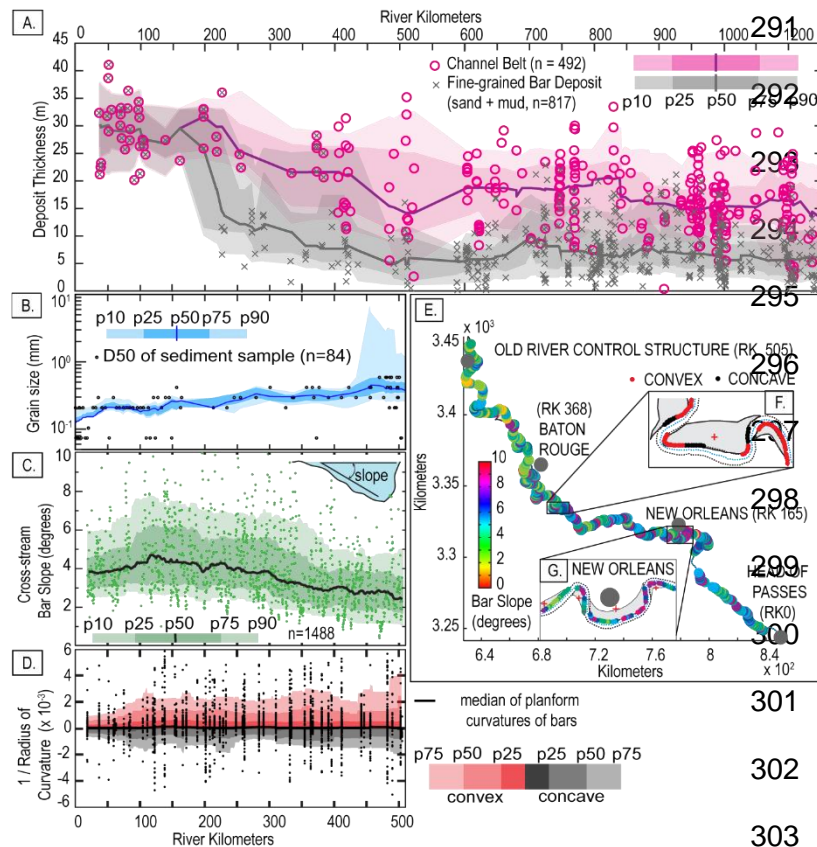
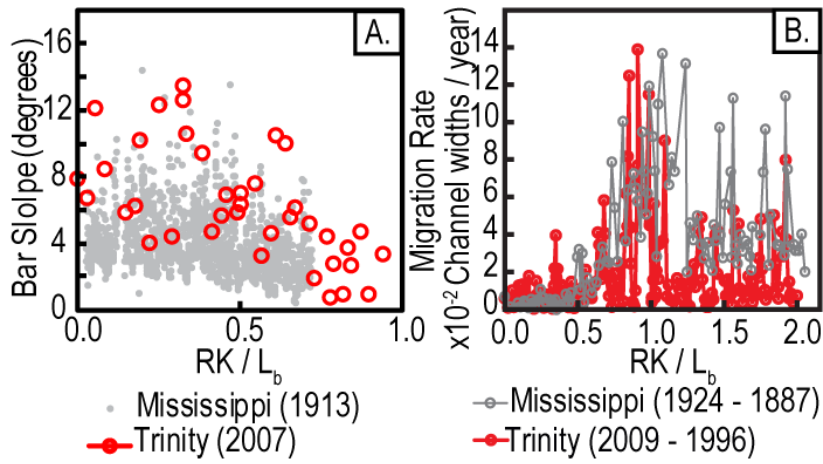


Figure 2: (A) Thickness of the channel belt and of Facies B from RK1200 to RK0. The 10th, 25th, 50th, 75th, 90th (p10, p25, p50, p75, p90) percentiles were calculated using a RK100 moving window. (B) Grain-size trends from bed material samples shown as the D50 (50th percentile of all nominal diameters) of the bed sample as well as the mean p10, p25, p50, p75, and p90 of all samples collected within a 50RK

304 window of the sample location. (C) Cross-stream slopes of bank-attached bars in degrees, as well as the
 305 p10, p25, p50, p75, and p90 of all measurements within a moving RK100 window. (D) The planform
 306 curvature of bars, expressed as convexity (positive values) and concavity (negative values). The median of
 307 all convex and concave curvatures in moving 100RK windows is given by the solid black line; the p25,
 308 p50, p75 of convex and concave shapes in 100RK windows are given by the red and grey envelopes
 309 respectively. (E) Spatial pattern in transverse slopes of bars. Insets (F and G) show details of the Late
 310 Holocene bar deposits (grey polygon), their centroids (red crosses), channel banks (black dotted lines) and
 311 channel centerline (blue dotted lines). (F) Detail of planform geometry at different points along the channel
 312 bank (G) Detail of measured mean slopes of the cross-stream bar surfaces.

313

314



315

316 Figure 3: Comparison of (A) cross-stream bar slopes and (B) lateral migration rates observed in the Lower
317 Mississippi and Trinity Rivers. Distance upstream of the river mouth is standardized by the backwater
318 length in both plots, and lateral migration rates in (B) are standardized by the mean channel width.

319